Light-Emitting Diodes

DOI: 10.1002/ange.201409518

Efficient Solid-State Light-Emitting CuCdS Nanocrystals Synthesized in Air**

*Ali Hossain Khan, Amit Dalui, Soham Mukherjee, Carlo U. Segre, D. D. Sarma, and Somobrata Acharya**

Abstract: *Semiconductor nanocrystals (NCs) possess high photoluminescence (PL) typically in the solution phase. In contrary, PL rapidly quenches in the solid state. Efficient solid state luminescence can be achieved by inducing a large Stokes shift. Here we report on a novel synthesis of compositionally controlled CuCdS NCs in air avoiding the usual complexity of using inert atmosphere. These NCs show long-range color tunability over the entire visible range with a remarkable Stokes shift up to about 1.25 eV. Overcoating the NCs leads to a high solid-state PL quantum yield (QY) of ca. 55% measured by using an integrating sphere. Unique charge carrier recombination mechanisms have been recognized from the NCs, which are correlated to the internal NC structure probed by using extended X-ray absorption fine structure (EXAFS) spectroscopy. EXAFS measurements show a Cu-rich surface and Cd-rich interior with 46% Cu^{I} being randomly distributed within 84% of the NC volume creating additional transition states for PL. Color-tunable solid-state luminescence remains stable in air enabling fabrication of light-emitting diodes (LEDs).*

Semiconductor nanocrystals (NCs) are promising candidates for color-tunable light-emitting diodes (LEDs) owing to their size, shape, and composition-dependent photoluminescence (PL) properties, photostability, and high PL quantum yields (QYs).[1–6] Recent progress in the synthetic strategies have led to the prospect of designing low-cost fabrication possibilities for high-efficiency LEDs using NCs as active light-emitting layer.[6–14] The active layer of NC-based LEDs is usually made from solution-processable routes which transform to the solid state within the device. Although most of the NCs are highly luminescent in solution form, the luminescence rapidly quenches in the solid state.[14–17] Thus, achieving intense solid-state luminescence from NCs is a key to enhance the efficiency of NC-based LEDs. Major challenges encountered in achieving solid-state luminescence from NCs are associated with self-absorption, nonradiative recombination pathways, and crystal size distribution that leads to energy transfer in solid proximity.[14–17] Consequently, it remains important to develop new strategies for designing efficient solid-state luminescent NCs by overcoming these detrimental phenomena.

Recent advances in ternary and quaternary alloyed semiconductor NCs have shown advantageous features, such as color-tunable PL, high PL QYs, and solution processability, showing prospects for fabricating LEDs.[18–25] Nevertheless, alloyed NCs show positional discontinuities of atoms at the surface and interior of NCs, the influence of which on the observed spectral transitions is largely unknown.[26] In addition, to the best of our knowledge, the design of solid-state-luminescent alloyed NCs of I-II-VI category has not been reported yet. Here we report on the synthesis of monodisperse ternary copper–cadmium–sulfide NCs simply by heating copper oleate and cadmium oleate with dodecanethiol in air without the inert atmosphere conventionally required for colloidal synthesis of NCs. These NCs readily show color-tunable PL over the entire visible spectrum with remarkably large Stokes shift. Overcoating the NCs with a CdS shell leads to a high solid-state PL QY of about 55%. These NCs show robust thermal and photostabilities sustaining nearly for a year. A novel carrier recombination mechanism is observed from the optical transitions which are correlated to the internal structure of NCs probed by using EXAFS spectroscopy. High solid-state PL QY enabled the fabrication of LEDs with NCs as active layer, with a remarkable low turn-on voltage. Electroluminescence (EL) obtained from the devices is stable over a wide range of operating voltages offering the possibility of meeting the technical requirements of NC-based LEDs.

We synthesized the NCs in a single step by mixing copper oleate, cadmium oleate, and 1-dodecanethiol in a molar ratio of 1:2:16 in the noncoordinating solvent 1-octadecene. The

[*] Dr. A. H. Khan, A. Dalui, Prof. D. D. Sarma, Dr. S. Acharya
Centre for Advanced Materials
Indian Association for the Cultivation of Science
Jadavpur, Kolkata 700032 (India)
E-mail: camsa2@iacs.res.in

S. Mukherjee, Prof. D. D. Sarma
Solid State and Structural Chemistry Unit
Indian Institute of Science
Bangalore 560012 (India)

Prof. C. U. Segre
Department of Physics & CSRRI, Illinois Institute of Technology
Chicago, IL 60616 (USA)

Prof. D. D. Sarma
Council of Scientific and Industrial Research—Network of Institutes for Solar Energy (CSIR-NISE)
New Delhi 110001 (India)

[**] This work was supported by the DST India. We thank N. Beaver and R. Obaid for EXAFS measurements. A.H.K and A.D. acknowledge CSIR, India. C.U.S. acknowledges the National Science Foundation's Materials World Network program, grant number DMR-086935. MRCAT operations are supported by the Department of Energy and the MRCAT member institutions. Use of the Advanced Photon Source at Argonne National Laboratory is supported by the U.S. Department of Energy, Office of Science, Office of Basic Energy Sciences, under contract number DE-AC02-06CH11357.

Supporting information for this article is available on the WWW under http://dx.doi.org/10.1002/anie.201409518.

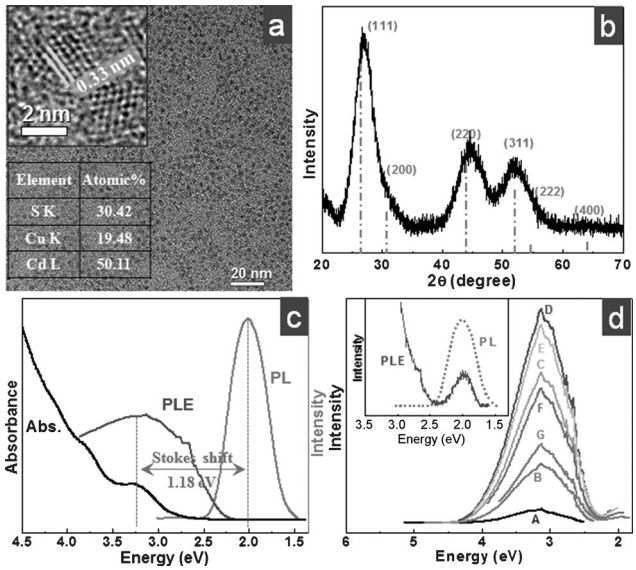

Figure 1. a) TEM images of CuCdS NCs. Top inset: HRTEM image. Bottom inset: elemental analysis by EDS in TEM. b) XRD pattern with reflections of zinc blende bulk CdS (dotted lines). c) UV/Vis absorption, PL (excitation 3.18 eV), and PLE (emission 2.0 eV) spectra of CuCdS NCs in chloroform solution. d) PLE spectra monitored at different emission energies (A, 2.431 eV; B, 2.296 eV; C, 2.175 eV; D, 2.006 eV; E, 1.068 eV; F, 1.878 eV; G, 1.796 eV). Inset: Comparison of PL (excitation 3.18 eV) and PLE (emission 1.55 eV) spectra showing overlap of the peaks at about 2 eV.

precursor mixture was annealed for 60 min at 200 °C in air (see the Supporting Information (SI) for details). The transmission electron microscopy (TEM) image shows monodisperse NCs with a diameter of 2.5 ± 0.2 nm (Figure 1 a). The high-resolution TEM (HRTEM) image shows that the NCs are single-crystalline in nature with well-resolved lattice spacing of 0.33 ± 0.02 nm corresponding to (111) planes of cubic bulk CdS (Figure 1 a, inset). Energy-dispersive X-ray spectroscopy (EDS) shows atomic ratios of 2:5:3 of Cu:Cd:S in the NCs suggesting a possible $Cu_2Cd_5S_3$ (hence onward denoted as CuCdS) cation-rich composition (Figure 1 a inset and Figure S1). Quantitative elemental analyses using inductively coupled plasma atomic emission spectroscopy (ICP-AES) support the observed atomic ratio for Cu to Cd cations. The TEM-EDS elemental analyses demonstrate sulfur deficiency in comparison to the cations in the resultant NCs. Powder X-ray diffraction (XRD) pattern of the NCs shows (111), (220), and (311) reflections corresponding to the zinc blende structure of bulk CdS (Figure 1 b). However, the XRD peaks are slightly shifted toward higher angles in comparison to a zinc blende CdS NCs of the same size suggesting that the reduced lattice spacing is possibly due to the incorporation of Cu within CdS (Figure S2).

The absorption spectrum of the NCs shows a peak at 3.18 eV, whereas the PL exhibits a peak at 2.0 eV implying a large Stokes shift of ca. 1.18 eV (Figure 1 c). The observed large Stokes shift can be accounted to the presence of Cu within CdS creating additional lower-energy transition states. One of the interesting features of the PL spectrum is the broad nature of the peak compared to the narrow PL peaks observed from binary NCs.[2,4,19] The PL excitation spectrum (PLE) shows a peak at 3.18 eV, at the same position as in the absorption spectrum (Figure 1 c). In addition, PLE measured by monitoring different energies of the broad PL peak show the same peak position (Figure 1 d), which suggests that the broadness of the PL peak is not related to the NCs size distribution. Interestingly, magnification of the spectral region between 1.77 eV and 2.48 eV of the PLE spectra shows another peak at about 2.0 eV, at the same position as the PL maximum (Figure S3 and Figure 1 d inset). The overlapping of PLE and PL peaks suggests common states of origin for both transitions at lower energies. The existence of two PLE peaks suggests the presence of separate energy states that contribute to the observed PL.

We have carried out X-ray photoelectron spectroscopy (XPS) to investigate the oxidation state of Cu within the NCs (Figure S4). A high-resolution XPS spectrum of Cu 2p state shows doublet peaks with a separation of 19.7 eV and the absence of any satellite features associated with $2p_{3/2}$ and $2p_{1/2}$ peaks are supportive of the presence of Cu^{I} state in the NCs. The 3d electrons of Cu may create two possible states: Cu^{I} ($3d^{10}$) and Cu^{II} ($3d^{9}$), among which the $3d^9$ is magnetically active.[27] We have performed electron paramagnetic resonance (EPR) measurements to identify the presence of unpaired electrons of Cu in the NCs. No EPR signal is observed for the NCs suggesting the absence of Cu^{II} states (Figure S5). However, control experiments with only the precursor mixtures (Cd, Cu-oleate) show EPR signals indicating paramagnetic behavior (Figure S5). Hence the Cu^{II} state, which is present in the precursor mixtures, is absent in the NCs due to the reduction of Cu^{II} to Cu^{I} by the ligands.[28]

The presence of Cu^{I} level indicates the possibility of isolated Cu^{I} state within the NCs when considered as dopant. Another possibility is the formation of chemical bonds with the CdS constituents forming an alloy. For an isolated Cu^{I} state, the PL will solely depend on the energy gap between the conduction band edge (CdS_{CB}) to the Cu^{I} level and the separation between Cu^{I} level and the valence band edge (CdS_{VB}) of the NCs will define the resultant Stokes shift observed in optical processes (Figure S6 and SI).[27] Hence, the energy gap between the Cu^{I} level and CdS_{VB} should be about 1.18 eV to match with the observed Stokes shift (Figure S6 b). However, our excitation-dependent PL measurements rule out the existence of an isolated Cu^{I} state within the NCs (Figure 2 a). The excitation energies spanning from 4.4 eV to 2.4 eV show the highest PL intensity for the 3.5 eV excitation which gradually decreases by lowering the excitation (Figure 2 a). Note that the PL maximum retains the same position for all excitation energies. Notably, the absorption spectrum showed a peak at 3.18 eV (Figure 1 c), whereas the PL can be obtained with excitation energies of up to 2.4 eV, which is below 3.18 eV. These optical measurements suggest the existence of additional energy levels within CdS_{VB} and CdS_{CB} creating a reduced energy gap for PL. Hence, the observed Stokes shift cannot be accommodated due to the presence of these additional states. On the other hand, alloying by chemical bond formation among the constituents may occur by substituting Cd^{II} atoms from the cubic CdS lattices or by the occupation at the interstitial positions of the

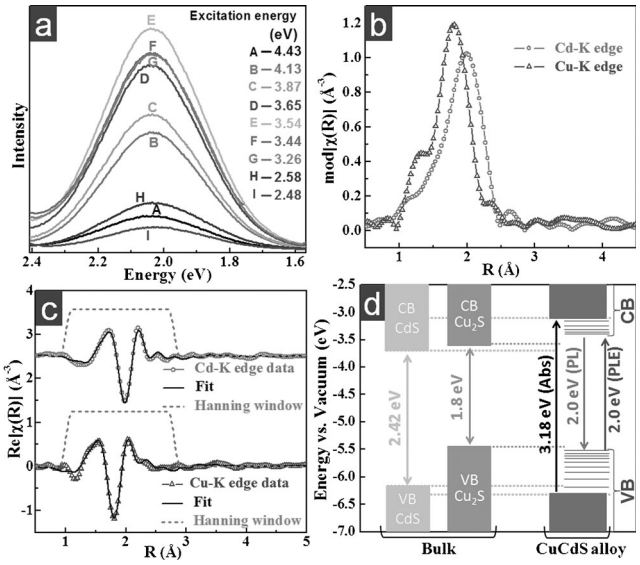

Figure 2. a) Excitation-dependent PL spectra of CuCdS NCs with excitation energies spanning from 4.4 eV to 2.4 eV. b) Overlay plots of *R*-space oscillations for both Cd-K and Cu-K edges for CuCdS NCs at 298 K. c) The real component of the *R*-space data and the corresponding fits (lines) to the Cd-K edge (open circles) and the Cu-K edge (open triangles) for CuCdS NCs. Hanning window over the fit range (1.0–2.8 Å) in *R*-space is shown by dotted lines. d) Schematic band diagram of bulk CdS, Cu_2S, and CuCdS NCs with the possible absorption, PL, and PLE pathways. The VB edges of both CdS and Cu_2S are kept at energies as near to bulk values considering their large hole effective masses,[32] whereas the CB edges are shifted to accommodate the confinement-induced band gap. Existence of additional $alloy_{CB}$ and $alloy_{VB}$ states in the NCs are marked by horizontal lines. The band gap of bulk CdS, Cu_2S, and the Cu state positions are collected from literature.[27,33]

CdS lattice by Cu^I. Both of these possibilities are feasible considering the ionic radii of Cd^{2+} (0.92 Å) and Cu^{1+} (0.74 Å). However, occupation of the interstitial positions would result in an excess of cations in the NCs, which perhaps is reflected by the elemental analyses showing distinct signature of anion deficiency.

We have probed the internal structure of NCs by EXAFS measurements at the Cu-K and Cd-K edges (SI). We extracted bond distances, coordination numbers, pseudo Debye–Waller factors, and energy shifts for relevant atom pair correlations using cubic CdS and $Cu_{1.95}S$ (F-43m) for modeling considering the extremities of alloy formation.[29,30] The dissimilarities in major frequency components between the k-space oscillations for the Cd-K and Cu-K edges of the NCs suggest different local atomic connectivities around the metal atoms (Figure S7). The magnitude of Fourier transforms (R-space oscillations) shows an apparent shortening of the bond distances (Figure 2b) corresponding to the well-known phase shift.[31] The real component of the R-space and the corresponding fits to the Cd-K and Cu-K edges for CuCdS NCs are shown in Figure 2c. Strikingly enough, we find that the local parameters of Cd closely match to cubic CdS, whereas the Cu–S distances appear ca. 0.3 Å shorter compared to Cd–S distances (Figure 2b) and the corresponding coordination number is lowered compared to an ideal tetrahedral environment (SI). We explored different possibilities such as cationic-site substitution by Cu in a CdS lattice, Cu occupation at interstitial positions, and surface precipitation to understand the local environment of NCs (SI). Additionally, we have accounted for the effect of metal–metal correlations (Cu–Cu, Cu–Cd, and Cd–Cd) and surface oxidation. The final model considers single scattering contributions from the closest near neighbor Cu–S and Cd–S correlations (Fit 1 and Fit 2, and Table S1 of the SI). Since the nearest atomic connectivities are strongly dictated by the local geometry, the shorter Cu–S distance can be well attributed to the smaller ionic radius of Cu^{1+} (0.74 Å) compared to Cd^{2+} (0.92 Å). The overall NC still maintains a global cubic symmetry with a Cd-rich core and a Cu-rich surface, thus lowering the Cu–S coordination number. On the other hand, Cd is residing largely in the interior maintaining tetrahedral connectivity in an ideal bulk cubic fcc lattice. Our final results indicate Cu as substitution impurity at the Cd sites, or occupying the S-coordinated high-symmetry interstitial sites, or both, residing largely near to the surface of the NCs.

Correlating the structural information from crystallography and the EXAFS results with analytical calculations, we calculated the fraction of Cu and Cd atoms in the core and surface assuming 4-S coordination in the core and 2-S coordination at the surface. We found a Cu-rich surface (76% Cu and 24% Cd) and a Cd-rich interior (12% Cu and 88% Cd), which clearly explains the lower bond distance and reduced coordination number for Cu–S correlations, whereas near-ideal Cd–S correlations were found for a cubic CdS. Our results suggest ca. 54% Cu^I residing at the surface, whereas the remaining Cu^I ($\approx$46%) participates in alloying within 84% of the entire NC volume defining a Cu-rich surface. Clearly, these results exclude the formation of a conventional core–shell NC structure. Additionally, small disorder (pseudo Debye–Waller factor values), low bond distance errors, and small energy shifts rule out the possibility of gradient alloy formation.[34] Hence we conclude that our NCs are inhomogeneous CuCdS alloys containing a dramatic difference of Cu to Cd ratio at the surface (3.2:1) and interior (0.14:1).

Hence the band structure of NCs should contain signatures of the alloyed states. However, the contribution from the interior will be CdS-dominated, whereas the contribution from surface will be Cu_2S-like considering the Cd-rich interior and Cu-rich surface. Based on this, we have modeled a band diagram with bulk CdS and Cu_2S while accounting the shift of the VB and CB edges of NCs due to the confinement effect accordingly to fit with the observed transition energies (Figure 2d and SI).[27] The band diagram shows the existence of alloyed states ($Cu_{alloy,VB}$ and $Cu_{alloy,CB}$) on the top of CdS_{VB} and below the CdS_{CB} (Figure 2d). Indeed the excitation-dependent PL spectroscopy (Figure 2a) showed the existence of energy states on the top of CdS_{VB} and/or below the CdS_{CB}. The absorption supposedly takes place from the states CdS_{VB}/$Cu_{alloy,VB}$ to CdS_{CB}/$Cu_{alloy,CB}$, whereas the PL originates from the $Cu_{alloy,CB}$ to $Cu_{alloy,VB}$ leading to two-level transition pathways distinct from a type-I band structure.[12] The absorption is governed by CdS states owing to the larger absorption cross section. One might expect two PLE peaks

for such a band structure corresponding to the excitation of electrons from CdS_{VB} and $Cu_{alloy,VB}$. Our emission-dependent PLE validates the band diagram (Figures 1 d and S3).

The resultant transition gap of alloyed NCs can be varied by changing the relative cationic ratio during the synthesis (Figure S8) or the annealing time (Figure 3 a–d). The absorption and PL spectra show a gradual redshift with increasing annealing time (Figure 3 a,b). The PL spectra of NCs at different annealing time show peaks with variable full-width at half-maximum ranging from 0.43 eV to 0.34 eV (Figure 3 b). Blue emission emerges at the initial stage of annealing, which evolves to red with longer annealing time eventually spanning the entire visible spectrum. The plot of absorption and PL maxima with annealing time shows an increment in the Stokes shift up to 1.25 eV (Figure 3 c). Such large Stokes shift is beneficial for avoiding self-absorption. Clearly the continuous change in Stokes shift differentiates our NCs from doped systems in which the dopant level remains fixed in the mid-gap region.[27] We have collected aliquots to quantify Cd to Cu ratios at different stages of annealing. ICP-AES results indicate a gradual variation of Cd to Cu ratio within the NCs showing a maximum for 90 min annealing (Figure 3 d). An increase in diameter from ca. 2 nm to ca. 3 nm is observed from TEM images for the longest annealed NCs (Figure S9). The XRD patterns of all annealed NCs show zinc blende structure with a shift toward smaller angles (Figure S9). Interestingly, the solution-phase absolute PL QY shows an optimal value of about 20 % for 60 min of annealing (Figure 3 d). Further annealing beyond 60 min results in a decrease of QYs. Hence, the continuous shift of the PL peak and variation of QY is associated with the change of composition and size of the NCs during annealing.[35] At the beginning of the reaction, Cd preferentially dominates over Cu and with annealing time Cu is eventually being ejected from the interior to the surfaces by a "self-purification" mechanism.[36] Longer annealing time promotes Cu residing at the surfaces to insert within the interior owing to the thermal energy decreasing the Cd to Cu ratio. The interplay of Cd to Cu ratio at different stages of reaction obviously creates intermediate states in the resultant alloyed NCs, which affects the recombination dynamics. Excited-state lifetimes of charge carriers by time correlated single photon counting (TCSPC) spectroscopy shows an increment in lifetimes with annealing reaching a maximum value of about 1 μs for orange-emitting NCs following the same trend with QY (Figure S10).

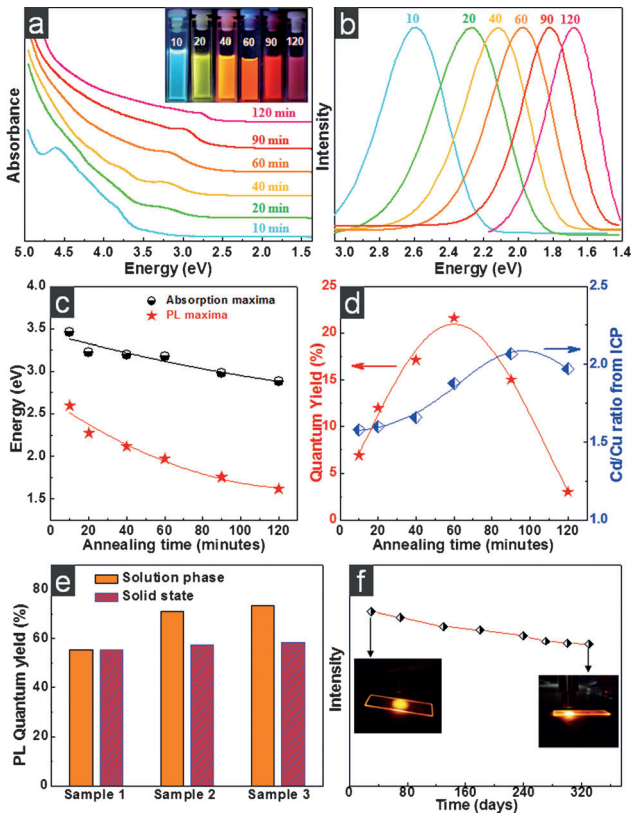

Figure 3. a) Absorption and b) PL spectra (excitation at 3.18 eV) of CuCdS NCs in chloroform at different stages of annealing. Inset of Figure (a): Digital photographs at different annealing time showing the true color with irradiation of 365 nm UV light. c) Spectral positions of the absorption maxima and the PL maxima and corresponding fits (black and red lines) with annealing time. (d) Dependence of PL QYs and Cd to Cu ratio (measured from ICP-AES) of CuCdS NCs with annealing time. e) Comparison of solution phase and solid-state PL QY of CuCdS/CdS core–shell NCs showing solid-state PL QY of 55 %. (f) Solid-state PL stability curve with time. Insets, photographs of solid state luminescence on quartz substrate and the arrows indicate corresponding days.

We further increased the QYs of alloyed NCs by overcoating a shell layer of CdS, which can simultaneously create an alloy with the NCs by forming a thin shell through diffusion at higher temperatures (Figure S11). To overcoat the alloyed NCs, TOP-S complex solution (0.1 mmol) and cadmium oleate (0.1 mmol) was added dropwise to the NC solution at 170 °C (SI). The absorption and PL spectra of the core–shell alloyed NCs show a blueshift of ca. 0.1 eV compared to the uncoated NCs, whereas retaining the same crystallographic structure (Figure S12). We have achieved a three-fold enhancement of solution-state PL QY by shelling the alloyed NCs, which readily gives solid-state luminescence with QY of about 55 % (Figure 3 e). Importantly, the solid-state PL traces the solution phase suggesting a minimized energy transfer within the NCs in the solid proximity (Figure S13 a). The solid-state PL stability has been monitored by checking the emission intensity with time, while keeping the alloyed NCs on a quartz substrate at ambient conditions. The stability plot shows that these NCs are substantially stable in air for nearly a year retaining bright solid-state luminescence (Figure 3 f). Thermogravimetric analysis indicates that the NCs are stable up to 250 °C proving their thermal robustness (Figure S13 b). In addition, the temperature-dependent PL measurement shows that the PL intensity is retained upon cooling down to room temperature suggesting that the luminescence is stable (Figure S13 c–e). The outstanding air and thermal stability together with the large Stokes shift and excellent PL tunability with high QY in the solid state further imply applicability of the ternary alloyed NCs in solid-state lighting.

To test the use of the alloyed NCs in fabricating LEDs, we designed LED devices by using alloyed NCs as active material

component. The simple device architecture contains orange color emitting core–shell NCs as active layer sandwiched in between TPD/PEDOT:PSS-coated indium tin oxide (ITO) anode and ZnO/Al cathode (Figure 4a). The current–voltage characteristics of the devices showed LED responses with an effectively low threshold voltage below ca. 2 V (Figure 4b).

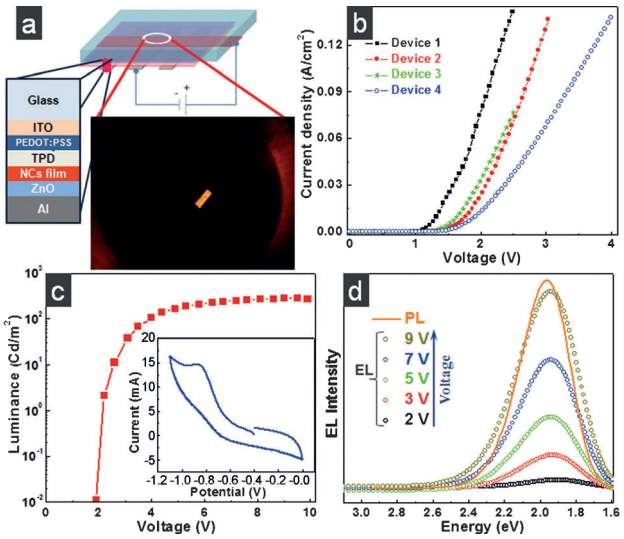

Figure 4. a) Device structure and photograph of a working LED at a driving voltage of 5 V showing uniform EL. The device is fabricated using CuCdS/CdS core–shell NCs annealed for 60 min. b) Current density versus voltage characteristics of different LED devices. c) Luminance characteristics of alloyed NCs LED at different voltages. Inset: Cyclic voltammetry curve of CuCdS/CdS NCs in N_2-purged dichloromethane solution at room temperature taken at a scan rate of 5 mVs^{-1}. d) EL spectra of the core–shell alloyed NC LEDs with increasing driving voltages. The PL spectrum (red line) matches with the EL spectra.

Above the turn-on voltage, the luminance–voltage plot is mostly linear in a double-logarithmic scale (Figure 4c). The cyclic voltammetry performed on core–shell NCs solution shows a low oxidation potential of 0.85 V (inset of Figure 4c), which may have caused the low turn-on voltage of the device. Luminance was detectable starting from a threshold voltage of 2 V showing a value of ~280 $Cd\,m^{-2}$ at 9 V with an external quantum efficiencies of 0.25% (Figures 4c and S14). The devices show bright and stable EL over a wide range of operating voltages (Figure 4d). The EL retraces the PL suggesting that the EL is occurring from the alloyed NCs (Figures 4d and S14c).

In summary, we have reported on the synthesis of new compositionally controlled CuCdS NCs in air. We demonstrate that the structure–property relationship dictates the recombination processes in ternary alloyed NCs. Overcoating these NCs with CdS results in high solid-state luminescence with high QYs. Our alloyed NCs have several attractive features for making them suitable candidates for solid-state lighting devices. First, the synthesis is carried out in air by simply annealing the precursor mixtures. This implies the mass-scale production possibilities by avoiding usual synthesis complexities and holds prospects for scaling up the device yield. Second, the alloyed NCs possess advantageous properties like a large Stokes shift and efficient solid-state luminescence, which are useful for fabricating LEDs. Third, NCs are stable in air for a year retaining high luminescent QY and good thermal stability. Fourth, the emission wavelengths are tunable, resulting in color control over the entire visible spectrum, a feature favorable for fabricating color-tunable LEDs. Although further scope remains for device engineering, our preliminary device fabrication shows a low turn-on voltage and bright EL within a range of operating voltages. We anticipate that the solid-state luminescence from the alloyed NCs will explore newer possibilities of similar classes of materials as a suitable candidate for LED fabrication.

Received: September 26, 2014
Published online: January 16, 2015

Keywords: alloys · colloid synthesis · EXAFS spectroscopy · fluorescence spectroscopy · light emitting diodes

[1] C. B. Murray, D. J. Norris, M. G. Bawendi, *J. Am. Chem. Soc.* **1993**, *115*, 8706–8715.
[2] L. H. Qu, X. G. Peng, *J. Am. Chem. Soc.* **2002**, *124*, 2049–2055.
[3] C. Burda, X. Chen, R. Narayanan, M. A. El-Sayed, *Chem. Rev.* **2005**, *105*, 1025–1102.
[4] I. Moreels, K. Lambert, D. Smeets, D. De Muynck, T. Nollet, J. C. Martins, F. Vanhaecke, A. Vantomme, C. Delerue, G. Allan, Z. Hens, *ACS Nano* **2009**, *3*, 3023–3030.
[5] C. She, A. Demortiere, E. V. Shevchenko, M. Pelton, *J. Phys. Chem. Lett.* **2011**, *2*, 1469–1475.
[6] D. V. Talapin, J.-S. Lee, M. V. Kovalenko, E. V. Shevchenko, *Chem. Rev.* **2010**, *110*, 389–458.
[7] V. L. Colvin, M. C. Schlamp, A. P. Alivisatos, *Nature* **1994**, *370*, 354–357.
[8] H. Mattoussi, L. H. Radzilowski, B. O. Dabbousi, E. L. Thomas, M. G. Bawendi, M. F. Rubner, *J. Appl. Phys.* **1998**, *83*, 7965–7974.
[9] S. Coe, W. K. Woo, M. Bawendi, V. Bulovic, *Nature* **2002**, *420*, 800–803.
[10] J. S. Steckel, P. Snee, S. Coe-Sullivan, J. P. Zimmer, J. E. Halpert, P. Anikeeva, L.-A. Kim, V. Bulovic, M. G. Bawendi, *Angew. Chem. Int. Ed.* **2006**, *45*, 5796–5799; *Angew. Chem.* **2006**, *118*, 5928–5931.
[11] A. L. Rogach, N. Gaponik, J. M. Lupton, C. Bertoni, D. E. Gallardo, S. Dunn, N. L. Pira, M. Paderi, P. Repetto, S. G. Romanov, C. O'Dwyer, C. M. S. Torres, A. Eychmueller, *Angew. Chem. Int. Ed.* **2008**, *47*, 6538–6549; *Angew. Chem.* **2008**, *120*, 6638–6650.
[12] B. N. Pal, Y. Ghosh, S. Brovelli, R. Laocharoensuk, V. I. Klimov, J. A. Hollingsworth, H. Htoon, *Nano Lett.* **2012**, *12*, 331–336.
[13] L. Sun, J. J. Choi, D. Stachnik, A. C. Bartnik, B.-R. Hyun, G. G. Malliaras, T. Hanrath, F. W. Wise, *Nat. Nanotechnol.* **2012**, *7*, 369–373.
[14] Y. Shirasaki, G. J. Supran, M. G. Bawendi, V. Bulović, *Nat. Photonics* **2013**, *7*, 13–23.
[15] T.-W. F. Chang, A. Maria, P. W. Cyr, V. Sukhovatkin, L. Levina, E. H. Sargent, *Synth. Met.* **2005**, *148*, 257–261.
[16] C. R. Kagan, C. B. Murray, M. Nirmal, M. G. Bawendi, *Phys. Rev. Lett.* **1996**, *76*, 1517–1520.
[17] J. Kundu, Y. Ghosh, A. M. Dennis, H. Htoon, J. A. Hollingsworth, *Nano Lett.* **2012**, *12*, 3031–3037.
[18] R. Xie, M. Rutherford, X. Peng, *J. Am. Chem. Soc.* **2009**, *131*, 5691–5697.
[19] M. D. Regulacio, M.-Y. Han, *Acc. Chem. Res.* **2010**, *43*, 621–630.

[20] S. Jun, E. Jang, *Angew. Chem. Int. Ed.* **2013**, *52*, 679 – 682; *Angew. Chem.* **2013**, *125*, 707 – 710.
[21] A. Singh, S. Singh, S. Levcenko, T. Unold, F. Laffir, K. M. Ryan, *Angew. Chem. Int. Ed.* **2013**, *52*, 9120 – 9124; *Angew. Chem.* **2013**, *125*, 9290 – 9294.
[22] H. Zhong, Z. Bai, B. Zou, *J. Phys. Chem. Lett.* **2012**, *3*, 3167 – 3175.
[23] B. Chen, H. Zhong, W. Zhang, Z. Tan, Y. Li, C. Yu, T. Zhai, Y. Bando, S. Yang, B. Zou, *Adv. Funct. Mater.* **2012**, *22*, 2081 – 2088.
[24] H. Shen, S. Wang, H. Wang, J. Niu, L. Qian, Y. Yang, A. Titov, J. Hyvonen, Y. Zheng, L. S. Li, *ACS Appl. Mater. Interfaces* **2013**, *5*, 4260 – 4265.
[25] Y. Zhang, C. Xie, H. Su, J. Liu, S. Pickering, Y. Wang, W. W. Yu, J. Wang, Y. Wang, J. Hahm, N. Dellas, S. E. Mohney, J. Xu, *Nano Lett.* **2011**, *11*, 329 – 332.
[26] S. Cadars, B. J. Smith, J. D. Epping, S. Acharya, N. Belman, Y. Golan, B. F. Chmelka, *Phys. Rev. Lett.* **2009**, *103*, 136802.
[27] R. Viswanatha, S. Brovelli, A. Pandey, S. A. Crooker, V. I. Klimov, *Nano Lett.* **2011**, *11*, 4753 – 4758.
[28] C. Corrado, Y. Jiang, F. Oba, M. Kozina, F. Bridges, J. Z. Zhang, *J. Phys. Chem. A* **2009**, *113*, 3830 – 3839.
[29] B. Ravel, M. Newville, *J. Synchrotron Radiat.* **2005**, *12*, 537 – 541.
[30] M. Newville, *J. Synchrotron Radiat.* **2001**, *8*, 322 – 324.
[31] B. K. Teo, *EXAFS: Basic Principles and Data Analysis*, Springer, Berlin, **1986**, pp. 26 – 27.
[32] L. E. Brus, *J. Chem. Phys.* **1984**, *80*, 4403 – 4409.
[33] A. Tang, F. Teng, Y. Wang, Y. Hou, W. Han, L. Yi, M. Gao, *Nanoscale Res. Lett.* **2008**, *3*, 502 – 507.
[34] P. K. Santra, R. Viswanatha, S. M. Daniels, N. L. Pickett, J. M. Smith, P. O'Brien, D. D. Sarma, *J. Am. Chem. Soc.* **2009**, *131*, 470 – 477.
[35] W. W. Yu, X. Peng, *Angew. Chem. Int. Ed.* **2002**, *41*, 2368 – 2371; *Angew. Chem.* **2002**, *114*, 2474 – 2477.
[36] G. M. Dalpian, J. R. Chelikowsky, *Phys. Rev. Lett.* **2006**, *96*, 226802.